

Structural characterization of a porous low-dielectric-constant thin film with a non-uniform depth profile

Eric K. Lin,^{a)} Hae-Jeong Lee, Gary W. Lynn,^{b)} and Wen-li Wu
Polymers Division, National Institute of Standards and Technology, Gaithersburg, Maryland 20899-8541

Mark L. O'Neill
Electronics Technology, Air Products and Chemicals, Inc., 7201 Hamilton Blvd., Allentown, Pennsylvania 18195

(Received 15 February 2002; accepted for publication 24 May 2002)

High-resolution x-ray reflectivity (XR) and small-angle neutron scattering (SANS) are applied to characterize both the nonuniform depth profile and pore structure of a low-dielectric-constant (low- k) thin film as prepared on a silicon substrate. The XR data show that the density depth profile has a multilayered structure with a dense, nonporous top layer and a less dense, porous bulk layer. A scattering invariant analysis of the SANS data is used to determine the average chord length of the pores, (14.8 ± 2.0) nm, independent of the depth profile. Given the elemental composition of the film, the XR and SANS data are combined to calculate the mass density of the top layer, (1.13 ± 0.05) g/cm³, the porosity of the less dense layer, (0.28 ± 0.10) , and the wall density, (0.92 ± 0.15) g/cm³. © 2002 American Institute of Physics. [DOI: 10.1063/1.1495079]

The semiconductor industry is rapidly developing new low dielectric constant (low- k) materials critical to continuing performance increases in integrated circuits. To lower the effective dielectric constant (k) to 2.0 and below, materials developers have identified new processes to incorporate pores or voids into a base material.¹ Many different strategies for accomplishing this have been pursued, including the introduction of thermally labile materials that are removed from the matrix by thermal post-treatments through the use of solvent mixtures,²⁻⁴ surfactant-templated structures,⁵ block copolymers⁶ or dendrimers.^{7,8} In addition, a large number of physical property requirements such as the Young's modulus and adhesion energy of the film must be met to ensure successful integration into standard silicon processing steps.¹

Unlike the nonporous conventional dielectric, silicon dioxide, the mesoscale structure of porous low- k dielectrics strongly influences the physical and electrical properties of the interlayer material. Characterizing the pore structure is critical to understanding the resulting material properties and to improving the fabrication process. There are few experimental techniques for on-wafer characterization of pore structure. They include positronium annihilation lifetime spectroscopy (PALS),⁹ ellipsometric porosimetry,¹⁰ and a combination of x-ray reflectivity (XR)¹¹ and small angle neutron scattering (SANS).^{12,13} To date, these methods have been applied to porous low- k films that have homogeneous density depth profiles, either assumed or measured. However, the dielectric film may have a nonuniform depth profile due to either processing or fabrication steps that complicates the analysis of the data from these characterization methods. For example, solid hydrogen silsesquioxane films have non-uniform density depth profiles after treatments with plasmas

designed to increase the surface density of the films and enhance their mechanical properties.¹¹

In this letter, we demonstrate the application of XR and SANS as a methodology to determine both the nonuniform depth profile of a porous thin film and information about the pore structure. Quantifying variations in the density profile is needed to correctly interpret the SANS data for the porosity, wall density, and pore size in the porous bulk of the film. A scattering invariant analysis of the SANS data is used to calculate the average pore size independent of the density depth profile. A full analysis of the XR and SANS data provides information consistent with a film structure with a porous lower layer covered by a layer of the nonporous matrix material.

The low- k dielectric film used in this study is a porous poly(arylene ether) film (Velox-ELKTM).¹⁴ The sample is prepared by spin-coating the resin from a solvent solution followed by spin-dispense of a nonsolvent developer. The choice of solvent and non-solvent strongly impacts the pore characteristics. In addition, a nonuniform depth profile arises from the application of the non-solvent developer solution. Specific details of the preparation methods for Velox-ELK can be found elsewhere.^{3,4} The mole fractions of the elements in the film are estimated from a combustion analysis of the base materials as $(57 \pm 5)\%$ carbon, $(40 \pm 5)\%$ hydrogen, and $(3 \pm 5)\%$ oxygen.¹⁵

High-resolution x-ray reflectivity at the specular condition (identical incident and detector angles, θ) was measured using a $\theta/2\theta$ configuration with a fine focus copper x-ray tube as the radiation source. The incident and reflected beams are both passed through germanium [220] monochromators. The resulting beam has a wavelength λ of 1.54 Å, a wavelength spread, $\Delta\lambda/\lambda = 1.3 \times 10^{-4}$, and an angular divergence of $12''$. This instrument has the precision and resolution necessary to observe interference oscillations in the reflectivity data from films up to 1.4 μm thick. The reflectivity data are plotted as a function of q [$q = (4\pi/\lambda)\sin\theta$].

^{a)}Electronic mail: eric.lin@nist.gov

^{b)}Current address: Oak Ridge National Laboratory, Oak Ridge, TN 37831-6430.

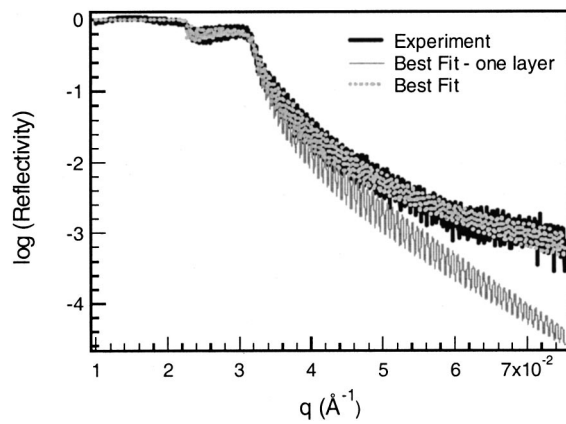


FIG. 1. X-ray reflectivity data from the porous low- k dielectric thin film as prepared on a silicon wafer along with the best fit to the data.

SANS measurements were performed on the 8 m NG1 line at the National Institute of Standards and Technology Center for Neutron Research. The neutron wavelength λ was 6 Å with a wavelength spread $\Delta\lambda/\lambda$ of 0.14. To increase the scattered intensity from these thin films, six sample pieces were stacked within the cell. The single crystal silicon substrates are nearly transparent to the neutron beam and the scattered intensity arises almost completely from the structure in the porous thin films. The two-dimensional scattering data were corrected for empty cell and background scattering using standard reduction methods. The scattered intensity was placed on an absolute intensity scale with reference to a neutron scattering standard. The scattered intensity is plotted as a function of q where $q = (4\pi/\lambda)\sin\theta$ and 2θ is the scattering angle.

In Fig. 1, the x-ray reflectivity from the film is presented as a function of q along with several fits to the data. At very low angles or q values, the x-ray radiation is almost totally reflected from the film surface with a reflectivity of unity. At a critical angle, θ_c , x rays begin to penetrate the top surface of the film. The critical angle is directly proportional to the electron density of the film near the top surface. At slightly higher q values near $q = 0.003 \text{ \AA}^{-1}$, another critical angle arising from the silicon substrate is visible. The oscillations in the reflectivity data represent the constructive and destructive interference between x-rays reflected from the film/air interface and the silicon/film interface as well as any other interfaces through the film.

In addition to the average mass density of the film, the film density depth profile and thickness can be determined from a detailed analysis of the reflectivity data. The x-ray reflectivity data are fit with a nonlinear least squares algorithm using the recursive multilayer method of Parratt.¹⁶ Model profiles are generated from multiple layers with varying thickness, electron density, and roughness. The best fit electron density depth profile to the data provides the overall film thickness, the film roughness, and the average electron density of the film.

An initial inspection of Fig. 1 does not immediately suggest a multilayered structure, because the reflectivity data appear to have a single frequency of oscillation. The best fit to the data using a single homogeneous layer is shown in Fig. 1 and clearly does not fit the experimental data. A full fit to the data requires five separate layers split into two general

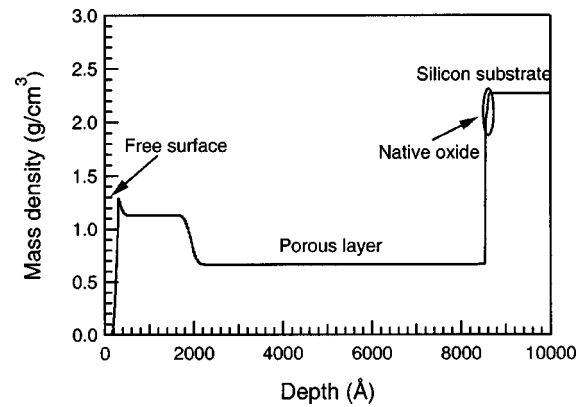


FIG. 2. The density depth profile of the porous thin film from the best fit to the x-ray reflectivity data. The elemental composition of the material is used to convert the electron density to a mass density.

sections, as shown in Fig. 2. There is a dense layer at the film/air surface and a less dense layer at the film/silicon substrate. The top layer is $(1670 \pm 10) \text{ \AA}$ thick with a density of $(1.13 \pm 0.05) \text{ g/cm}^3$, a reasonable value for an organic material. The lower layer of the film has a density of $(0.66 \pm 0.05) \text{ g/cm}^3$ with a thickness of $(6620 \pm 10) \text{ \AA}$. The interfacial width between these two layers is approximately 200 Å. From this data, there is not significant variation in porosity through the porous region of the film because the average mass density of the porous part of the film is uniform. The XR data, however, are insufficient to determine if the pore size distribution varies through the layer. These observations are qualitatively consistent with scanning electron microscopy images of the film cross section.

The average mass density of the film ρ_{eff} is related to the porosity and wall density of the film through Eq. (1):

$$\rho_{\text{eff}} = \rho_w(1 - P), \quad (1)$$

where ρ_w is the density of the wall material and P is the porosity of the film. Here, an assumption of the matrix mass density could provide a numerical estimate of the film porosity, but not pore size. Equation (1) also assumes that the film is homogeneous but is easily generalized for any position in a varying density depth profile.

Figure 3 shows the raw SANS data on an absolute intensity scale assuming that all of the scattering objects (pores) are located in the lower layer of the film. The scattering thickness is taken to be 6620 Å, the thickness of the less dense layer. The data show the intensity decreasing strongly with increasing q . From the log-log plot, the limiting power law behavior follows the Porod limiting scaling law, $I \sim q^{-4}$, shown in Fig. 3. This limit indicates that the pore/wall interface is smooth and not fractal.¹⁷ The plateau in the data at higher q values comes from the background incoherent scattering primarily from the hydrogen in the sample. The background intensity is determined to be $(0.35 \pm 0.1) \text{ cm}^{-1}$ and is subtracted from the data before performing the following analysis.

To determine the average chord length, ℓ_c , or pore size from the SANS data, we apply an invariant analysis for the analysis of small angle scattering from a two-phase system.¹⁸ This approach has the advantage of determining ℓ_c of a two-

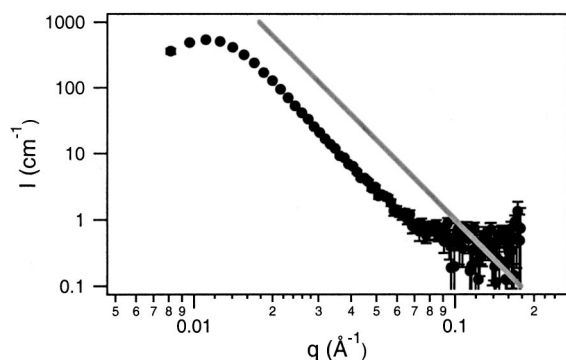


FIG. 3. Small angle neutron scattering data plotted on a log-log scale as a function of q . The data are placed on an absolute intensity scale using a scattering volume of the porous lower layer of the film. The limiting Porod power law scaling, $I \sim q^{-4}$, is also shown by the solid line.

phase system from SANS data without reference to an absolute intensity scale. The scattering invariant of the SANS data is given by

$$Q_{\text{exp}}^* = \int_0^{\infty} q^2 I(q) dq. \quad (2)$$

Conceptually, the invariant relates the experimental intensity to the average mean square of the scattering length fluctuations.¹⁹ The measured invariant can be used to directly determine the average chord length ℓ_c through

$$\ell_c = \frac{\pi}{Q_{\text{exp}}^*} \int_0^{\infty} q I(q) dq. \quad (3)$$

This approach assumes that there are only two phases in the system with sharp interfacial boundaries ($I \sim q^{-4}$), conditions that are met in this sample. The Porod power law ensures that the integrals in Eqs. (2) and (3) converge. From the SANS data, ℓ_c is (14.8 ± 2.0) nm, a value consistent with those from PALS measurements.⁹ Errors in ℓ_c , however, may arise because the SANS data fall over a limited q range. The SANS data may be extrapolated to higher q following the Porod power law behavior, but the scattering at lower q values (higher intensity) is not known because of practical instrumental limitations. However, it is expected that significant errors would arise only if there was a significant fraction of large pores (>500 nm).

To determine the porosity of the film using this formalism, we use the theoretical definition of the invariant given by the equation

$$Q_{\text{th}}^* = 2\pi^2 \Delta \rho_N^2 P(1-P) = Q_{\text{exp}}^* \quad (4)$$

As in the Debye two-phase model, there are two equations, Eq. (1) and Eq. (4), which are functions of ρ_w and P (given the elemental composition). Here, the absolute scattering intensity is important because a ratio is not used to determine the porosity and wall density. The porosity and the wall density are calculated to be (0.28 ± 0.10) and (0.92 ± 0.15) g/cm³, respectively.

The structural parameters for the film calculated using the scattering invariant approach can be compared with the values from the Debye two-phase calculation to provide a

more consistent interpretation of the XR and SANS results. For a given scattering volume, the Debye formalism assumes a random two-phase structure.¹² Using this model dependent calculation, the lower layer porosity, pore wall density, and average chord length are determined to be (0.36 ± 0.2) , (1.04 ± 0.35) g/cm³, and (20 ± 7) nm, respectively. The relatively large error in these parameters arises from the small error bars in the SANS intensity and the imperfect fit of the scattering data to the Debye model (random two-phase). The invariant calculation for this case is more accurate because it does not depend upon the assumption of a scattering model. However, the results from both analyses are consistent with a film structure with fully dense top layer forming approximately 20% of the overall film thickness and a porous bottom layer with an average pore chord length ℓ_c of about 15 nm. The XR data used to determine the depth profile of the film were critical toward the proper interpretation of the SANS data. These results demonstrate that the application of both XR and SANS measurements can provide quantitative, detailed information about the structure of porous low- k dielectric thin films even with nonuniform density depth profiles.

¹M. Morgen, E. T. Ryan, J. H. Zhao, C. Hu, T. Cho, and P. S. Ho, *Annu. Rev. Mater. Sci.* **30**, 645 (2000).

²T. A. Deis, C. Saha, E. Moyer, K. Chung, Y. Liu, M. Spaulding, J. Albaugh, W. Chen, and J. Bremmer, in *Materials, Technology, and Reliability for Advanced Interconnects and Low-k Dielectrics*, edited by K. Maex, Y.-C. Joo, G. S. Oehrlein, S. Ogawa, and J. T. Wetzel (Materials Research Society Meeting, San Francisco, CA, 2001), Vol. 612, Paper D5.18.

³M. L. O'Neill, L. M. Robeson, T. J. Markley, X. Gao, M. Langsam, D. A. Roberts, S. Motakef, and P. R. Sierocki, in *Proceedings of the Sixteenth International VMIC Conference Santa Clara, CA, 1999*, p. 92.

⁴M. L. O'Neill, L. M. Robeson, W. F. Burgoyne, and M. Langsam, US Patent No. 6,187,248 (13 February 2001).

⁵A. Sellinger, P. M. Weiss, A. Nguyen, Y. F. Lu, R. A. Assink, W. L. Gong, and C. J. Brinker, *Nature (London)* **394**, 256 (1998).

⁶S. Yang, P. Mirau, C. S. Pai, O. Nalamasu, E. Reichmanis, E. K. Lin, H. J. Lee, D. W. Gidley, and J. N. Sun, *Chem. Mater.* **13**, 2762 (2001).

⁷C. V. Nguyen, C. J. Hawker, R. D. Miller, E. Huang, J. L. Hedrick, R. Gauderon, and J. G. Hillborn, *Macromolecules* **33**, 4281 (2000).

⁸J. Bolze, M. Ree, H. S. Youn, S. H. Chu, and K. Char, *Langmuir* **17**, 6683 (2001).

⁹T. L. Dull, W. E. Frieze, D. W. Gidley, J. N. Sun, and A. F. Yee, *J. Phys. Chem. B* **105**, 4657 (2001).

¹⁰M. R. Baklanov, K. P. Mogilnikov, V. G. Polovinkin, and F. N. Dultsev, *J. Vac. Sci. Technol. B* **18**, 1385 (2000).

¹¹H. J. Lee, E. K. Lin, W. L. Wu, B. M. Fanconi, J. K. Lan, Y. L. Cheng, H. C. Liou, Y. L. Wang, M. S. Feng, and C. G. Chao, *J. Electrochem. Soc.* **148**, F195 (2001).

¹²W. L. Wu, W. E. Wallace, E. K. Lin, G. W. Lynn, and C. J. Glinka, *J. Appl. Phys.* **87**, 1193 (2000).

¹³E. Kohdoh, M. R. Baklanov, E. K. Lin, D. W. Gidley, and A. Nakashima, *Jpn. J. Appl. Phys.* **40**, L323 (2001).

¹⁴Certain commercial equipment and materials are identified in this paper to specify adequately the experimental procedure. In no case does such identification imply recommendation by the National Institute of Standards and Technology nor does it imply that the material or equipment is necessarily the best available for this purpose.

¹⁵All data in the manuscript and in the figures are presented along with the standard uncertainty of the measurement.

¹⁶L. G. Parratt, *Phys. Rev.* **95**, 359 (1954).

¹⁷H. D. Bale and P. W. Schmidt, *Phys. Rev. Lett.* **53**, 596 (1984).

¹⁸Th. Zemb in *Neutron, X-ray, and Light Scattering: Introduction to an Investigative Tool for Colloidal and Polymeric Systems*, edited by P. Lindner and Th. Zemb (North Holland, Amsterdam, 1991), p. 177.

¹⁹G. Porod, *Zolloid-Z.* **124**, 83 (1951).